Applied Catalysis B: Environmental 254 (2019) 206–213

Contents lists available at ScienceDirect

Applied Catalysis B: Environmental

journal homepage: www.elsevier.com/locate/apcatb

Carbonate-intercalated defective bismuth tungstate for efficiently photocatalytic NO removal and promotion mechanism study

Wangchen Huo[a,b], Weina Xu[c], Tong Cao[a], Xiaoying Liu[d], Yuxin Zhang[a,*], Fan Dong[b,*]

[a] State Key Laboratory of Mechanical Transmissions, College of Materials Science and Engineering, Chongqing University, Chongqing 400044, PR China
[b] Research Center for Environmental Science & Technology, Institute of Fundamental and Frontier Sciences, University of Electronic Science and Technology of China, Chengdu 611731, PR China
[c] Department of Physics, Chongqing University, Chongqing, 401331, PR China
[d] Engineering Research Center for Waste Oil Recovery Technology and Equipment, Ministry of Education, College of Environment and Resources, Chongqing Technology and Business University, Chongqing 400067, PR China

ARTICLE INFO

Keywords:
Carbonate intercalated
Oxygen vacancy
Bi_2WO_6
Photocatalytic NO removal
DFT

ABSTRACT

Synthesis of high-efficiency photocatalysts and revealing the photocatalytic mechanism are of far-reaching significance for its commercial applications. Therefore, we design and favorably fabricate the carbonate intercalated Bi_2WO_6 with oxygen vacancies via employing a mild hydrothermal method with ethylene glycol assist. The prepared catalysts exhibit an excellent photocatalytic NO oxidation activity under visible light irradiation, attributing to the inserted carbonate coupled with oxygen vacancies. Additionally, the promotion mechanism and reaction pathway of photocatalytic NO removal are carefully discussed by experimental detection assisted with density functional theory (DFT) calculation. Our results explicitly reveal that the carbonate coupled with oxygen vacancies can remarkably retard the recombination of electro-hole pairs, and improve the carriers transforming to activity species. The reactants would be easily activated and converted over the carbonate-intercalated defective Bi_2WO_6 surface, such as the H_2O provided electrons to form $^{\cdot}OH$ and O_2 accepted electrons to generate $^{\cdot}O_2^-$, which are certified by utilizing DFT simulation to calculate adsorption of reactants on the surface. In addition, the *in situ* DRIFTS spectra was used to dynamic analyze the photocatalytic NO oxidation process and reveal the promotion mechanism. Finally, the synthesis strategy and mechanism analysis would possess guiding significance for improving photocatalytic efficiency and applications.

1. Introduction

Currently, semiconductor photocatalytic technology has attracted enormous interest and been regarded as an extremely promising methods for efficiently harvesting solar energy to relieve the urgent issues about environment pollution and energy shortage [1], such as, CO_2 reduction [2], water splitting [3], nitrogen fixation [4] and NO oxidation [5,6] et al. In general, the photocatalytic reaction process could be concluded by the following three steps: i) reaping solar energy to produce electron-hole pairs; ii) the separation and transformation of carrier to form the activity specific; iii) the redox reaction on the surface of catalysts [1,7,8]. Therefore, developing the photocatalysts with wide light absorption range, low recombination rate of carriers, high generation rate of reactive radical and stable surface structure, are of far-reaching significance for improving the photocatalytic efficiency and its commercial applications.

Among diversiform photocatalysts, Bi-based photocatalytic materials such as $Bi_{12}O_{17}C_{l2}$ [9], BiO_{2-x} [10], BiOBr [4], $BiVO_4$ [3] and Bi_2WO_6 [11] et al. have received good graces from numerous researchers, due to the superior activity under visible light and preferable potential applications in practice [2,9,10,12]. Specially, as one of the famous Bi-based photocatalysts, bismuth tungstate (Bi_2WO_6) exhibits a promising potential to meet the high-efficiency photocatalytic application, owning to the desirable visible light absorption, peculiar alternating layer structure for facilitating electron-hole separation and transformation, good thermal stability and eco-friendliness [12,13]. However, the Bi_2WO_6 photocatalysts always could not meet the requirement of highly and robustly photocatalytic activity in engineering application, due to the sluggish electron-hole separation ratio, depressed reactive radical conversion, and inferior ability to activate reactants over the surface [13]. Thus, in order to settle these shortcoming and promote the photocatalytic efficiency in application, a series of structure tuning and modifying strategies based on the above-mentioned three aspects have been developed, such as synthesizing

* Corresponding authors.
E-mail addresses: zhangyuxin@cqu.edu.cn (Y. Zhang), dfctbu@126.com (F. Dong).

https://doi.org/10.1016/j.apcatb.2019.04.099
Received 25 February 2019; Received in revised form 16 April 2019; Accepted 30 April 2019
Available online 01 May 2019
0926-3373/

ultrathin nanosheets [2], introducing oxygen vacancies [14] and doping heteroatoms [15] et al. In details, Yi Xie et al. [2] found that the routes can enhance the solar-driven CO_2 reduction activity via fabricating single unit cell Bi_2WO_6 layers structure, owning to the unique structure favoring carrier transport and increasing carriers' lifetime. Zhu et al. [14] reported that the Bi_2WO_{6-x} nanoplates show the good light response ability and high performance, which is caused by the existence of oxygen vacancies enhancing the light absorption. Wang et al. [15] claimed that the iodide inserted into Bi_2WO_6 layers exhibit an excellent photocatalytic activity under visible light, because of the doping iodide would promote charge separation and prohibit the recombination. These examples elucidate that the strategies could efficiently promote the photocatalytic efficiency via enhancing light absorption and facilitating carrier separation, while the further photocatalytic reaction mechanism about the active species and reactants activation is still a challenge. Therefore, developing the carbonate intercalated in Bi_2WO_6 with oxygen vacancies could be a feasible and valid route to heighten photocatalytic performance and expedite commercial applications, meanwhile revealing the reaction radical and reaction pathway during the photocatalytic process is meaningful and worthwhile.

Herein, we design and successfully synthesize the carbonate-intercalated defective Bi_2WO_6 photocatalysts by utilizing a facile one-pot ethylene glycol assisted hydrothermal method. The prepared catalysts exhibit a superior photocatalytic NO oxidation performance than the "perfect" catalysts under visible light irradiation. Additionally, the promotion mechanism and NO oxidation process are carefully investigated from various perspectives, including light absorption, carrier recombination, reactive species, activation of reactants and the reaction process over time, by *in situ* experimental characterization methods assisted with DFT simulation. Interestingly, the presence of oxygen vacancies could improve the harvesting visible light, electro-hole separation and conversion to reaction radical, oxidation of H_2O and reduction of O_2. More importantly, carbonate-intercalated defective Bi_2WO_6 could further enhance the aforementioned characteristics, except the visible light absorption, in addition this routes could improve the oxidation of NO over the surface. The strategy to fabricate catalysts and promotion mechanism analysis could provide guiding significance for synthesis of high-efficiency photocatalysts and its commercial applications.

2. Methods

2.1. Raw materials

All chemicals applied in this work are the analytical purity, which could be directly utilized without any further purification. Sodium tungstate dehydrate ($Na_2WO_4{\cdot}2H_2O$, ≥99.0%), sodium carbonate (Na_2CO_3, ≥98.0%), and bismuth nitrate pentahydrate ($Bi(NO_3)_3{\cdot}5H_2O$, ≥98.0%) were purchased from Alfa Aesar. Ethanol (C_2H_5OH, Grade AR 96.0%) and ethylene glycol (EG, ≥99.0%) were purchased from Chongqing Chuandong Chemical (Group) co. LTD, China.

2.2. Synthesis of photocatalysts

The carbonate-intercalated defective Bi_2WO_6 has been favorably synthesized by employing the facile one-step EG-assisted solvothermal method. In details, 3 mmol $Bi(NO_3)_3{\cdot}5H_2O$ was mixed into 20 mL EG solution under stirring and labeled A. Meanwhile, 1.425 mmol $Na_2WO_4{\cdot}2H_2O$ and 0.075 mmol Na_2CO_3 were dissolved in 10 mL EG solution under stirring and labeled B. After A and B completely dissolved, then B was dropt into A under mighty magnetic stirring for 1 h. Then the mixture was sealed into a 50 mL Teflon-lined autoclave, heated at 160 °C for 18 h. After the reaction finished, the precipitates were washed with water and ethanol to remove residual species on the surface of products, and dried at 60 °C for overnight. The products with highly oxygen vacancy (VO) defects was named as 5% − CO_3-BWO-VO. In addition, the carbonate-intercalated Bi_2WO_6 without defects was prepared via a simple annealing process, which is the 5% − CO_3-BWO-VO calcined at 400 °C for 4 h under air-rich atmosphere, the products marked with 5% − CO_3-BWO.

Similarly, the control experiment is set by adjusting the rate of Na_2CO_3 and $Na_2WO_4{\cdot}2H_2O$ (0: 1.5, 0.045: 1.5, 0.15: 1.5), and repeat the aforementioned procedure. The products are named as BWO-VO, BWO, 3% − CO_3-BWO-VO, 3% − CO_3-BWO, 10% − CO_3-BWO-VO and 10% − CO_3-BWO, respectively.

2.3. Materials characterization

The characteristics about structure and morphology were investigated by utilizing the focused ion beam scanning electron microscope (Zeiss Auriga FIB/SEM) and transmission electron microscope (TEM, ThermoFisher Scientific, Talos F200S). The information of chemical composition and crystal structure were verified via employing the X-ray diffraction (Cu Ka, Rigaku D/max 2500), Raman spectrum (LabRAM HR Evolution) and elemental analyzer (Vario EL cube). The surface chemical state was surveyed by X-ray photoelectron spectroscopy (XPS, ESCALAB250Xi, Al Ka). The electron paramagnetic resonance (EPR) and electron spin resonance (ESR) measurement was detected by Bruker JES FA200 spectrometer equipped with xenon lamp as visible light source. DMPO (5, 5′-dimethyl-1-pirroline-*N*-oxide) was qualified as a spin-trap reagent to test the hydroxyl ($^{\cdot}OH$) and superoxide radicals ($^{\cdot}O_2^-$). The UV–vis diffuse-reflectance spectra (UV-2700, Japan) and Hitachi F4600 fluorescence spectrophotometer (PL) were applied to investigate the optical properties, and $BaSO_4$ served as the reflectance sample. Based on the UV–vis spectra, the band gaps of prepared samples were calculated as the previous study [12]. In details, the band gaps are estimated by the formula $\alpha h\nu = A(h\nu - E_g)^{\eta/2}$, the α is the absorption coefficient, h is the Planck constant, A is a constant and E_g is the absorption bandgap energy, and the coefficient η is 4 due to the indirect bandgaps. In addition, *in situ* diffuse reflectance infrared Fourier transform spectroscopy (DRIFTS) measurements as reported before [5,12], were employed to dynamic monitor the reaction pathway of photocatalytic NO oxidation. And in this work, we have employed the continuous stream method to investigate the photocatalytic NO oxidation process. In details, the mixture gas (50% NO and 50% O_2) is continuing through the detection chamber of *in situ* DRIFTS measurement during the adsorption and oxidization process, where the adsorption process is before light on while the oxidization process is after light on, which method could dynamic detect the reaction process and investigate the accumulation of intermediate and final products.

2.4. Photocatalytic activity measurement

The method of evaluating photocatalytic NO removal and equipment are the same with our previous work [16]. The detailed procedure, the photocatalytic activities of prepared catalysts were assessed by monitoring the efficiency of NO removal in the 4.5 L (30 × 15 × 10 cm) rectangular reactor with continuous flow at ambient environment. The prepared photocatalyst (0.20 g) was dispersed in ethyl alcohol with assistance of ultrasonic wave and uniformly covered on two glass culture dishes with a diameter of 12.0 cm, then dried at 60 °C. Continuously, the dishes place at the reactor center after naturally cooling to room temperature. The initial NO was diluted with air stream from 100 ppm (balance N_2) to about 550 ppb. The mass flow controller tuned the flow rates of the NO (15 mL min^{-1}) and air stream (2.4 L min^{-1}), then the NO and air streams were premixed well utilizing a three-way valve. After achieving adsorption-desorption equilibrium, the tungsten halogen lamp (150 W) vertically placed on the reactor with UV cutoff filter (λ ≥ 420 nm) provided visible light was light on. At every min, the concentration of NO was recorded on the NO_x analyzer (Thermo Scientific, model 42c-TL). The NO removal

efficiency (η) was calculated from $\eta = (1 - C/C_0) \times 100\%$, where C_0 and C are the NO concentrations in the inlet and outlet, respectively.

2.5. Density functional theory calculations

The calculations have been ran on Vienna ab-initio simulation package (VASP5.4) via applying density functional theory (DFT) with projector augmented wave (PAW) pseudopotential [17–20]. Generalized gradient approximation (GGA) has been performed for exchange correlation functional to carry out the periodic calculations [21,22]. Moreover, a plane wave cutoff of 500 eV was employed, k-points was sampled with the 8 × 3 × 8 Monkhorst-Pack grid, and the force of atom convergence was set as 0.01 eV/Å [5]. The DFT + U method applied in strong correlation systems was used to calculate the density of state (DOS), and the U values were set to 5 and 5 eV corresponding the Bi and W, respectively [23]. A 1 × 1 × 2 supercell of perfect Bi_2WO_6 was relaxed, and then carbonates were brought into substitute tungstates (**Schematic S1, Supplementary material**). Additionally, three layers slabs (108 atoms) cut along the (131) facets, and the vacuum thickness was 15 Å.

3. Results and discussions

The carbonate-intercalated defective Bi_2WO_6 catalysts were synthesized using ethylene glycol as solvent. The solvent possess the reducibility could induce the oxygen vacancies (VOs) into crystal structure of photocatalysts to form the defective catalysts. Moreover, the carbonate inserted in deficient catalysts is well-tuned by controlling the ratio of raw materials. A detailed description of the synthesis procedure is given in the Methods. The morphologies and structural information of the prepared photocatalysts were characterized by the FIB/SEM and TEM. The SEM micrographs show that all photocatalyst nanostructures aggregate together, although the 5% − CO_3-BWO-VO displays the partial perpendicular nanosheets as well as the 3% − CO_3-BWO-VO and 10% − CO_3-BWO-VO (Figs. 1a-d and S1). The aggregation can be ascribed to the extremely tiny nanostructures, as presented in the TEM images (Fig. 1x-1), the prepared samples (BWO, BWO-VO, 5% − CO_3-BWO and 5% − CO_3-BWO-VO) are composed of 10~30 nm ultrathin nanosheets. Additionally, the corresponding HRTEM information of the prepared catalysts are exhibited in (Fig. 1x-2), where x = a, b, c and d. The lattice spacing of BWO, BWO-VO, 5% − CO_3-BWO and 5% − CO_3-BWO-VO is respectively corresponding the 0.316, 0.319, 0.316 and 0.318 nm, which match well with that of Bi_2WO_6 (131), suggesting that both trifling carbonate intercalated and defects induced in bismuth tungstate could maintain the well-defined crystal structures. However, the lattice spacing of defective catalysts (with oxygen vacancies) is slightly larger than that "prefect" catalysts (without oxygen vacancies), which could own to the presence of oxygen vacancy defects in crystal lattices resulting in portion distortion [4,12].

Confirming the formation of oxygen vacancies in prepared catalysts via solvothermal routes is necessary and meaningful. The electron paramagnetic resonance (EPR) measurement was applied to elucidate the defective features (Fig. 2a). EPR spectra demonstrate that the 5% − CO_3-BWO-VO and BWO-VO exhibit a noticeable signal at the g-value of 1.9998, verifying the existence of oxygen vacancies in crystal structure [10]. However, the fingerprint signal is very weak in the BWO, even disappeared in the 5% − CO_3-BWO, which indicates the absence or just a little of oxygen vacancies in their structure. This results clearly show the prepared samples with rich defects in crystal structure.

To further investigate information about the crystal structure of the photocatalysts, the XRD (Figs. 2b and S2a) and Raman spectrums (Fig. 2c) were employed. All diffraction peaks are well indexed to the Russellite Bi_2WO_6 (PDF#39-0256) without foreign peaks, suggesting that the carbonates are favorably inserted in bismuth tungstate crystal structure without another impurity phase. Besides, the information about the lattice vibration was verified by Raman spectrum. Due to the absence of O atoms in crystal lattices, the Raman fingerprints of BWO-VO and 5% − CO_3-BWO-VO are not clearly presented, but the fingerprints can be confirmed from the catalysts without defects. In details, the bands center at 792 and 824 cm^{-1} are severally assigned to the antisymmetric and asymmetric vibration of O—W—O [15], while the center

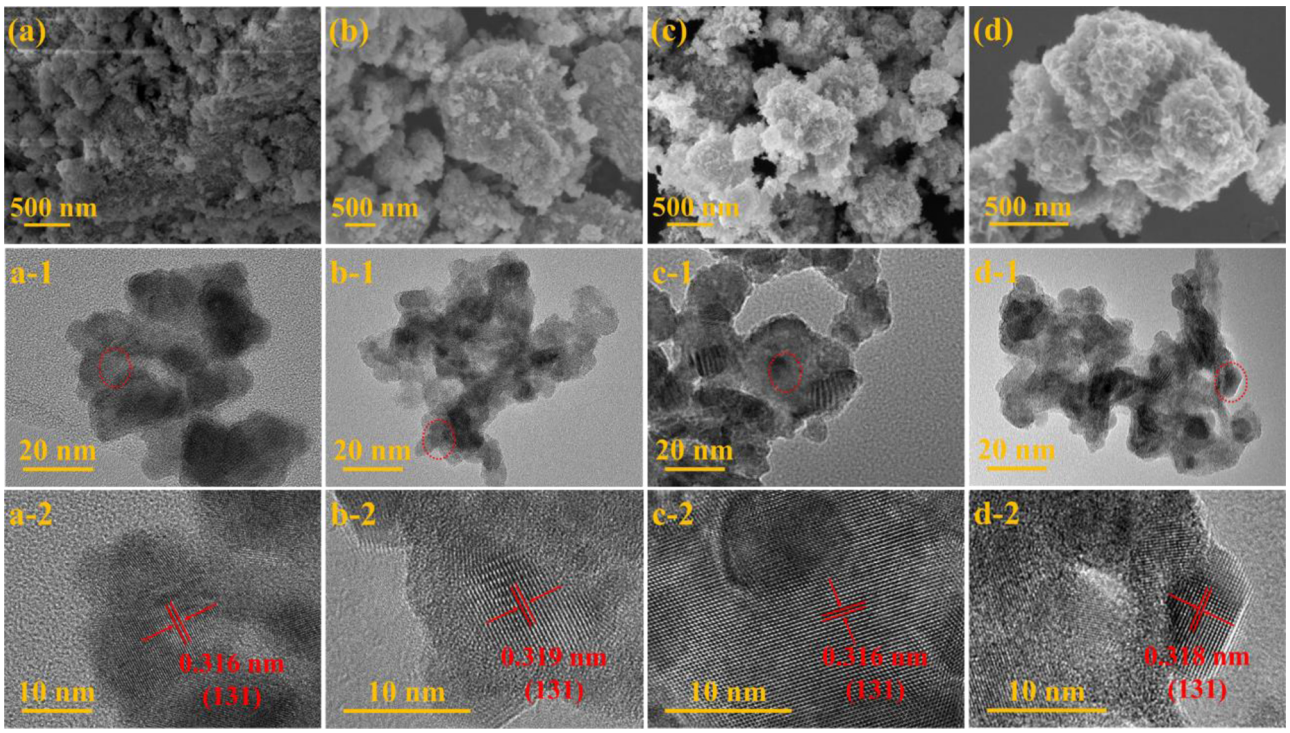

Fig. 1. SEM (x), TEM (x-1) and the corresponding HRTEM images (x-2) of the BWO (a), BWO-VO (b), 5% − CO_3-BWO (c) and 5% − CO_3-BWO-VO (d), where x = a, b, c and d.

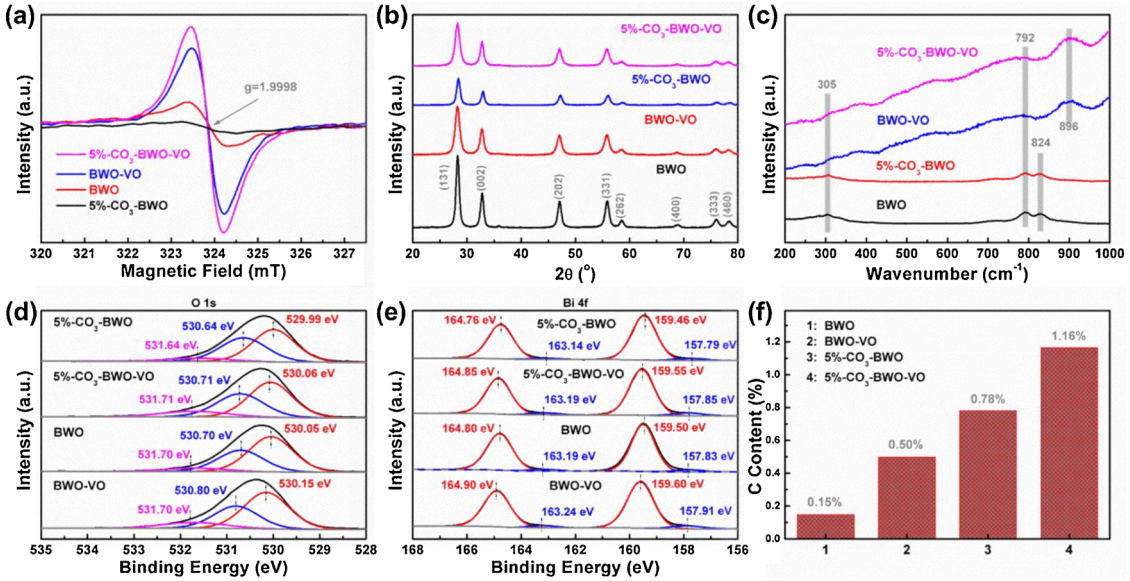

Fig. 2. XRD patterns (a), Raman spectrums (b), high-resolution XPS spectra of O 1s (c) and Bi 4f (d), EPR spectra (e) and quantitative analysis of carbon elements (f) of the BWO, BWO-VO, 5%−CO_3-BWO and 5%−CO_3-BWO-VO.

located at 305 cm^{-1} could be ascribed to bending vibration of Bi-O [15,24]. In addition, the broad band at 896 cm^{-1} appears in the curves of BWO-VO and 5%−CO_3-BWO-VO, which is ascribed to vibration of the shortest W−O bond caused by the oxygen vacancies [25].

Meanwhile, the XPS spectra was applied to analyze the surface chemical state of prepared photocatalysts and deeply discuss the surface properties of carbonate-intercalated defective Bi_2WO_6. The survey XPS spectrums of BWO, BWO-VO, 5%−CO_3-BWO and 5%−CO_3-BWO-VO affirm that the four prepared-catalysts are constituted by Bi, W, O, and a trace amount of carbon (Fig. S2b). For the BWO and BWO-VO, the carbon elements are absolutely ascribed to the surface chemisorbed carbon from ambient. However, the carbon of 5%−CO_3-BWO and 5%−CO_3-BWO-VO is partial chemisorbed carbon, and mainly the inserted carbonate. Based on the high-resolution O 1 s spectrum of 5%−CO_3-BWO-VO (Fig. 2d), the asymmetric peak could be fitted by three bands at 530.06, 530.71 and 531.71 eV, which are assigned to the different oxygen coordination, respectively corresponding the Bi-O bond, W−O bond and adsorbed oxygen [11,14]. Similarly, high resolution O 1 s spectra of the other catalysts has the same coordination of oxygen. In addition, it is clearly to observe that the two main deconvoluted peaks (Bi−O and W−O) of the catalysts with oxygen vacancies have a 0.07 eV left shift (between 5%−CO_3-BWO-VO and 5%−CO_3-BWO) and 0.10 eV left shift (between BWO-VO and BWO), owing to the sites neighbouring oxygen vacancies with stronger electron trapping ability [26]. At the same time, the intensity of adsorbed oxygen peak could reflected the concentration of oxygen vacancy as an assistant [26]. The adsorbed oxygen peak of the catalysts with defects is noticeable increased by comparing with "perfect" catalysts, accompanying the slightly decreasing of Bi-O peaks. This implies that the photocatalysts synthesized by solvothermal method possess the oxygen vacancies via releasing lattice oxygen from Bi-O bond.

Therefore, the atomic physicochemical state of Bi was characterized and analyzed by the high resolution Bi 4f spectrum (Fig. 2e). The two main peaks of 5%−CO_3-BWO-VO at 164.85 and 159.55 eV can be owned to the Bi $4f_{5/2}$ and Bi $4f_{7/2}$ in the Bi^{3+} chemical state, respectively [11]. Moreover, the two additional weak peaks located at 163.19 and 157.85 eV suggest the presence of $Bi^{(3-x)+}$ owning to the partial reduction of Bi chemical state by releasing lattice oxygen [26]. By comparing the defective catalysts and "perfect" catalysts, the intensity of peaks referred the $Bi^{(3-x)+}$ chemical state for defective catalysts is faintly higher than another, implying the generation of oxygen vacancy in crystal structure. Besides, the appearing of $Bi^{(3-x)+}$ chemical state in "perfect" catalysts (BWO and 5%−CO_3-BWO) could be resulted from the imperfect crystal, such as still containing the extremely tiny oxygen vacancies (demonstrate in above-mentioned paragraph about ESR) and carbonate substituted the tungstate. Additionally, the main peaks of defective catalysts have a 0.06 eV left shift (between 5%−CO_3-BWO-VO and 5%−CO_3-BWO) and 0.10 eV left shift (between BWO-VO and BWO) compared with "perfect" catalysts, which the reason is similar with the high resolution O 1 s spectra and the analogous shift (0.08 eV) are also appeared in the high resolution W 4f spectra (Fig. S2c). From the W 4f spectrum of 5%−CO_3-BWO-VO, the main peak center at 37.93 and 35.79 eV can be vested in the W $4f_{5/2}$ and W $4f_{7/2}$, respectively [11]. Finally, the C 1 s high resolution spectra of 5%−CO_3-BWO-VO shows in the Fig. S2d, the peaks located at 288.68, 286.33 and 284.82 eV stand for the C=O, C–O and C–C bond, respectively [27]. The C=O and C−O intensity of 5%−CO_3-BWO-VO and BWO-VO is obviously higher than two other catalysts, which is due to the stronger carbonate adsorption ability with the presence of oxygen vacancy. Although the survey XPS spectra and quantitative XPS analysis (Table S1) confirm the presence of carbon elements in the prepared photocatalysts, it cannot directly certify that the carbonates are successfully intercalated into the defective catalyst. Hence, quantitative analysis of carbon elements (Fig. 2f) was carried out Vario EL cube (elemental analyzer, analytical precision of C element < 0.2%). The content of carbon elements in difference prepared photocatalysts is increased in order of BWO (0.15%) < BWO-VO (0.50%) < 5%−CO_3-BWO (0.78%) < 5%−CO_3-BWO-VO (1.16%). The carbon elements emerged in BWO could not verify the existence of carbon, because of the carbon content is lower than analytical precision. For BWO-VO, due to the stronger adsorption ability resulted from the existence of oxygen vacancies, therefore, the detected carbon content could be attributed to adventitious adsorbed carbon on the surface. Similarly, the partial carbon in 5%−CO_3-BWO-VO would be provided by the adventitious carbon. And the 0.78% carbon can be confirmed in 5%−CO_3-BWO, suggesting the carbon species favorably induced in the prepared sample. These aforementioned results can sufficiently certify that the carbonates are successfully intercalated in the Bi_2WO_6 catalysts with rich oxygen vacancy defects.

Based on the prepared photocatalysts, the photocatalytic NO oxidation was employed to estimate the photocatalytic activity of the prepared samples. As Figs. 3a and S3 shows, the all NO removal curves

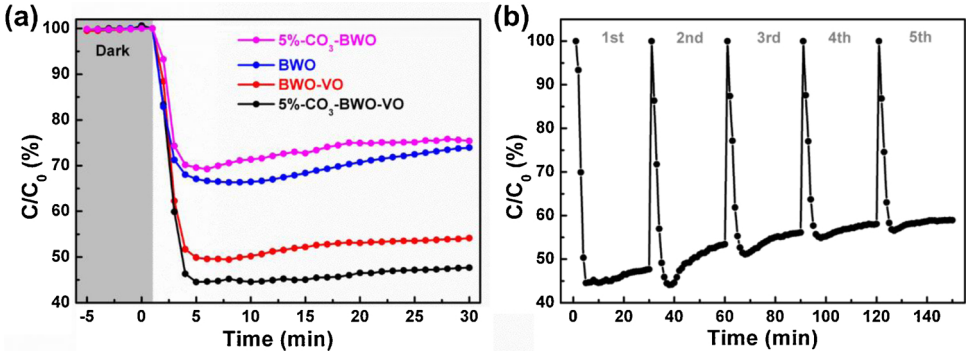

Fig. 3. NO removal curves of the BWO, BWO-VO, 5%−CO_3-BWO and 5%−CO_3-BWO-VO under irradiation of visible light (a). Cycling runs for the photocatalytic NO removal over 5%−CO_3-BWO-VO under visible light irradiation (b), the catalysis was not washed to remove the nitrate on the surface after each cycles.

reach the maximum purification ratio at ca. 5 min under visible light irradiation. More importantly, the 5%−CO_3-BWO-VO exhibits the highest NO removal ration (˜55%) than other catalysts, and thus, its catalytic stability was investigated by utilizing the five consecutive cycles (Fig. 3b). After five unremitting cycles, the curves have a recovery, which can be ascribed to the accumulation of final products (nitrates), thus occupying the reaction active sites on surface and delaying the photocatalytic reaction rate, but the catalyst still maintains an excellent and stabilized photocatalytic activity (˜42%). The strategy of carbonates intercalated defective Bi_2WO_6 catalysts would significantly improve the photocatalytic efficiency for NO oxidation. However, the promotion mechanism and NO oxidation process are not clear, but which are significance and worthy of study for catalytic reaction.

Therefore, the light absorption, carrier recombination, reactive species, activation of reactants and the reaction process over time were employed to investigate the promotion mechanism and NO oxidation process via combining the DFT calculation performed on VASP. Firstly, the optical traits of the prepared photocatalysts were characterized by utilizing the UV–vis spectra (Figs. 4a, b and S4a, b) and PL spectra (Figs. 4c and S4c). The photocatalysts with defects show a superior light absorption ability than “perfect” samples, and the corresponding estimated band gaps are smaller. Interestingly, the 5%−CO_3-BWO-VO with best photocatalytic activity put up a weaker ability of light absorption and wider band gap than BWO-VO, implying that carbonate induced in defective Bi_2WO_6 could not enlarge the light absorption range. However, the PL spectra of 5%−CO_3-BWO-VO shows that the preferable performance, suggesting that the inserted carbonate would effectively prevent the rapid recombination of photogenerated electron-hole pairs. Moreover, the electronic structure of catalysts was also illustrated by employing the DFT calculation. From the density of state (DOS), the conduction band (CB) edge and valence band (VB) edge are mainly contributed by the O 2p and W 5d, respectively (Fig. 4d and S4d-f). And the band gaps of these structure calculated by DFT are well-agreed with the variation tendency of estimated gap. Above-mentioned results demonstrate that the appearance of oxygen vacancies would not also enhance the light absorption, but also decrease the electron-hole recombination. More importantly, the introduced carbonate mainly inhibits the electron-hole recombination rather than the enlarging the light absorption range.

Secondly, the reactive species produced in the photocatalytic reaction process were distinguished by electron spin resonance (ESR) measurement with DMPO as spin-trap reagent, which is used to measure the hydroxyl (˙OH) and superoxide radicals ($˙O_2^-$). As shown in Fig. 4e, the four pairs of ESR signals with intensities of 1:2:2:1 (*) are emerged after the visible light on, and the intensity of these antisymmetric peaks is observably strengthened with increasing of illumination time, revealing the formation of ˙OH and sharply increaseing after light

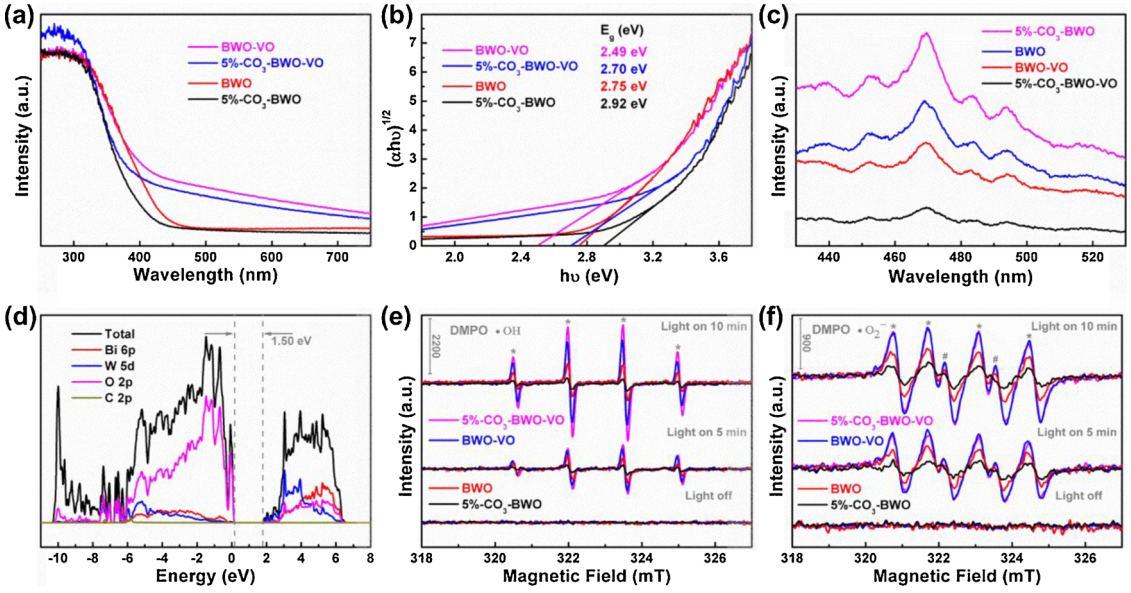

Fig. 4. UV–vis diffuse reflectance spectra (a), the estimated band gaps (b) and PL spectra (c) of the BWO, BWO-VO, 5%−CO_3-BWO and 5%−CO_3-BWO-VO. Density of state (DOS) of CO_3-BWO-VO (d) was calculated by employing the DFT + U methods. ESR spectra of DMPO-˙OH (e) and DMPO-$˙O_2^-$ (f) for the BWO, BWO-VO, 5%−CO_3-BWO and 5%−CO_3-BWO-VO in darkness and under visible light irradiation.

on [28]. Significantly, the specific signal intensity of 5% − CO_3-BWO-VO is stronger than others, while the 5% − CO_3-BWO is weakest, which indicate that the carbonate coupled with oxygen vacancies would dramatically improve the generation of ˙OH. Similarly, the fingerprint ESR signals with intensities of 1:1:1:1 (the four main peaks, *) are observed with the irradiation, while the other two tiny peaks (#) are resulted from the $DMPO^+$ regents (Fig. 4f), certifying the production of $^{\cdot}O_2^-$ [5]. The intensity of 5% − CO_3-BWO-VO is much the same with BWO-VO and higher than others, implying that oxygen vacancies would promote the $^{\cdot}O_2^-$ formation. In addition, the H_2O (gas) and O_2 are the reactants in photocatalytic NO oxidation process. Thus, combining the ESR results, the main active species are the hydroxyl and superoxide radicals during the photooxidation process over the 5% − CO_3-BWO-VO under visible light irradiation, whilst reveal that carbonate coupled with defects would facilitate the photoinduced electron-holes transformation to reactive radicals.

To further illustrate the transformation process of active species, the reactants activation was investigated by analyzing the adsorption of reactants over the surface of different catalyst models. The activation of the H_2O (g), O_2 and NO reactants over the different models calculated by DFT methods are presented in Fig. 5. The Bader effective charge difference of different reactants was calculated following the formula: $\Delta q = q_{ads} - q_{iso}$, where the q_{ads} and q_{iso} are Bader charge of the reactant adsorbed on catalyst surface and isolated species. It can be clearly seen that a bond length (l_{H-O1}) of H_2O (g) adsorbed on CO_3-BWO-VO surface is larger than other models, and the other one (l_{H-O2}) maintains a stable configuration, which is favor of producing ˙OH. Moreover, the Bader effective charge difference of H_2O (g) on CO_3-BWO-VO is lowest (-0.051 e) with maximum absolute value, which the negative value indicates that the CO_3-BWO-VO surface would promote H_2O molecules losing electrons, implying the H_2O as electron donor can be easier transformed to ˙OH. And maximum absolute value certifies the strongest ability. Similarly, the bond length (l_{O-O}) and Bader effective charge difference of O_2 adsorbed on CO_3-BWO-VO surface is longest (1.505 Å) and highest (1.140 e), respectively. These confirm that the O_2 molecules as electron acceptor can be easier converted to $^{\cdot}O_2^-$. These results about activation of H_2O and O_2 sufficiently verify that carbonate coupled with oxygen vacancies can prominently accelerate the reactants transforming to reactive radicals, which are well agreement with the preceding results about active species. In addition, bond length (l_{N-O}) of the other reactant (NO) over the CO_3-BWO-VO surface is also the longest (1.759 Å), which is favor of the NO oxidization. The corresponding Bader effective charge difference is lower than BWO-VO, but higher than others. Interestingly, the Bader effective charge difference of CO_3-BWO is lowest, suggesting that carbonate intercalated in catalysts can suppress the NO accepting electrons, thus promoting the oxidation of NO reactants.

Finally, the time-dependent DRIFTS spectra was applied to visually

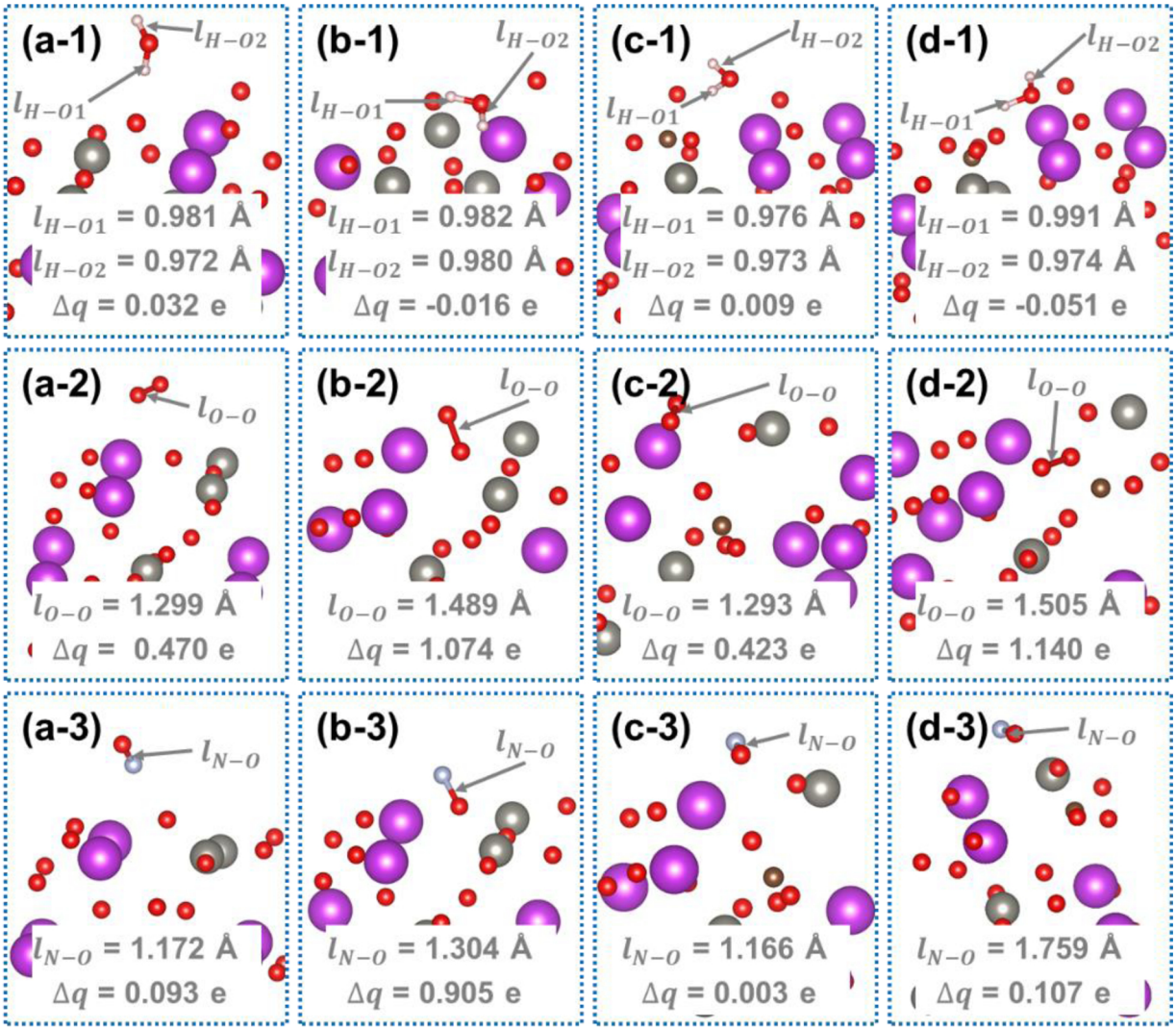

Fig. 5. The activation of the H_2O (x-1), O_2 (x-2) and NO (x-3) reactants over the surface of the BWO (a–n), BWO-VO (b–n), CO_3-BWO (c–n) and CO_3-BWO-VO (d–n), where x = a, b, c and d, whilst the n = 1, 2 and 3. l is the bond length and the Δq is the Bader effective charge difference.

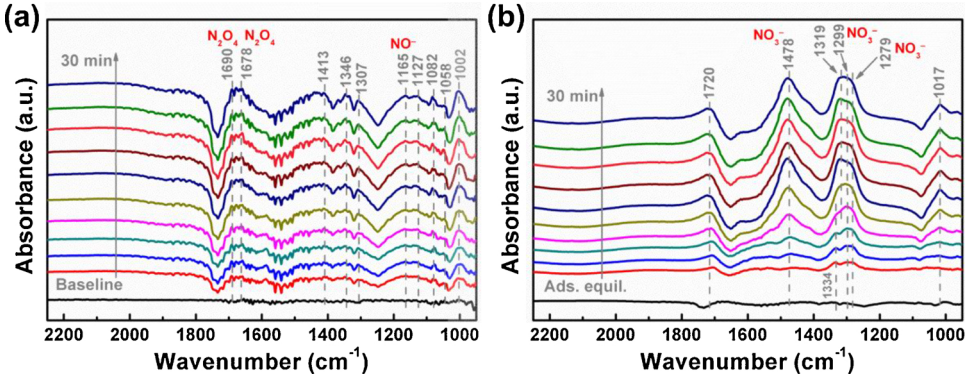

Fig. 6. in situ DRIFTS spectra of NO adsorption (a) and oxidization processes (b) under visible light illumination over the 5% − CO_3-BWO-VO.

Table 1
Assignment of the *in situ* DRIFTS bands observed on the surface of 5% − CO_3-BWO-VO.

Wavenumbers (cm^{-1})	Assignment	References
1002, 1058, 1017, 1307, 1299	Bidentate nitrate, $\nu(NO_3)$	[12,30,33,34,36,37]
1082	Line nitrites, $\nu(NO_2)$	[35]
1127, 1165	NO^-	[29,35]
1279, 1478	Monodentate nitrate, $\nu(NO_3)$	[12,31,32,37]
1346, 1413, 1334	Bridge nitrites, $\nu(NO_2)$	[12,33]
1319	Bridge nitrate, $\nu(NO_3)$	[35]
1678, 1690	N_2O_4	[30]
1720	Nitrosyls compounds	[12,29]

inquiry the photocatalytic NO removal reaction process, including the intermediate and final products during the primary reaction. As shown in Fig. 6a, the curves over time are recorded the adsorption process of NO on the photocatalyst surface in the dark condition. The baseline curve is first detected before the mixture gas containing NO flowing into reaction chamber. Evidently, there are many adsorption bands arising and enhancing with the time, which bands could ascribed to the adsorbed species of NO, and the detailed assignment of these bands are presented in Table 1. The main bands in adsorption process are the 1165 and 1678 cm^{-1}, which are respectively assigned to the NO^- and N_2O_4 [29,30], suggesting the NO mainly transformed to NO^- and N_2O_4. In addition, after reaching the adsorption equilibrium (Ads. equil.), the curves continuously monitor the oxidization processes of NO under visible light irradiation (Fig. 6b). The bands center at 1279, 1299, 1319 and 1478 cm^{-1} are appeared and rapidly increased with the increasing of illumination time, which bands can be respectively ascribed to monodentate nitrate, bidentate nitrate, bridge nitrate and monodentate nitrate [12,31–35], indicating that the main final products are the nitrate. Interestingly, at the preliminary stage of illumination, the band center at 1334 cm^{-1} emerges, which can be owned to the vibration of bridge nitrites [12], and the band is subsequently disappeared with illumination time, revealing that the generation of nitrites is one of the primary reaction steps to from intermediates, not the final products. Moreover, the in situ DRIFTS spectra of BWO, BWO-VO and 5% − CO_3 BWO were also measured (Fig. S5) and the corresponding assignment was presented in Table S2. Therefore, combining all of the aforementioned results and analysis, the primary NO oxidation reaction mechanism can be described by utilizing the below equations (1~7), whilst the schematic of reaction pathway is presented in Fig. 7.

$$\text{photocatalysts} + h\nu \rightarrow h^+ + e^- \quad (1)$$

$$h^+ + H_2O \rightarrow H^+ + \bullet OH \quad (2)$$

$$e^- + O_2 \rightarrow \bullet O_2^- \quad (3)$$

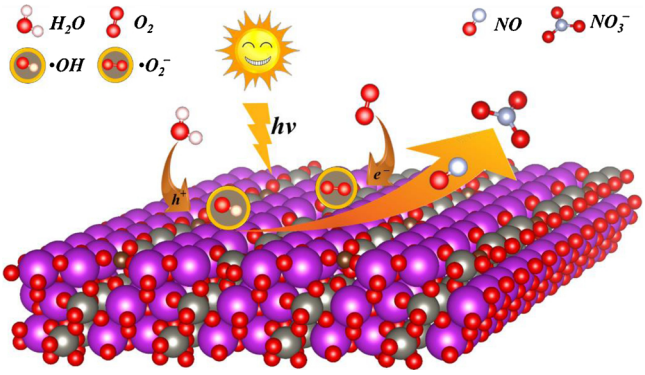

Fig. 7. The schematic of photocatalytic NO oxidation reaction pathway.

$$NO + \bullet O_2^- \rightarrow NO_2^- \quad (4)$$

$$NO + \bullet OH \rightarrow HNO_2 \quad (5)$$

$$NO_2^- + \bullet HO \rightarrow HNO_3 \quad (6)$$

$$HNO_2 + \bullet O_2^- \rightarrow HNO_3 \quad (7)$$

4. Conclusions

In summary, the carbonate-intercalated defective Bi_2WO_6 synthesized by one-pot hydrothermal route with EG assist shows an outstanding photocatalytic NO removal activity under visible light illumination, owning to the inserted carbonate and induced oxygen vacancy defects. The existence of defects were confirmed by using EPR measurement, meanwhile the carbonate was verified via elemental analyzer. In addition, the promotion mechanism is deeply discussed by analyzing the light response, electro-hole recombination ratio, active species and reactants activation. Interestingly, the carbonate coupled with oxygen vacancies in Bi_2WO_6 catalysts can observably reduce the electron-hole recombination, rather than enhance the light response ability. At the same time, the carbonate coupled with defects can facilitate the electron-hole pairs converting to reaction radical and reactants activation, including the H_2O oxidized to $^{\cdot}OH$, O_2 reduced to $^{\cdot}O_2^-$ and the oxidation of NO. Additionally, the time-dependent DRIFTS spectra was applied to dynamic monitor the intermediate and final products in the photocatalytic NO oxidation process. Based the results over time, the photocatalytic reaction pathway is also proposed. Finally, the promoting photocatalytic activity strategy and reaction process study are of significance for synthesis of high-efficiency photocatalysts and its commercial applications.

Acknowledgments

This work supported by the Fundamental Research Funds for the Central Universities (2018CDYJSY0055 and 106112017CDJXSYY0001), the National Natural Science Foundation of China (Grant no. 21576034), Joint Funds of the National Natural Science Foundation of China-Guangdong (Grant no. U1801254), the project funded by Chongqing Special Postdoctoral Science Foundation (XmT2018043), and Technological projects of Chongqing Municipal Education Commission (KJZDK201800801). The authors thank the Electron Microscopy Center of Chongqing University for Materials Characterizations.

Appendix A. Supplementary data

Supplementary material related to this article can be found, in the online version, at doi:https://doi.org/10.1016/j.apcatb.2019.04.099.

References

[1] T.M. Su, Q. Shao, Z.Z. Qin, Z.H. Guo, Z.L. Wu, Role of interfaces in two-dimensional photocatalyst for water splitting, ACS Catal. 8 (2018) 2253–2276.
[2] L. Liang, F. Lei, S. Gao, Y. Sun, X. Jiao, J. Wu, S. Qamar, Y. Xie, Single unit cell bismuth tungstate layers realizing robust solar CO_2 reduction to methanol, Angew. Chem. Int. Ed. Engl. 54 (2015) 13971–13974.
[3] C.W. Dong, S.Y. Lu, S.Y. Yao, R. Ge, Z.D. Wang, Z. Wang, P.F. An, Y. Liu, B. Yang, H. Zhang, Colloidal synthesis of ultrathin monoclinic $BiVO_4$ nanosheets for Z-Scheme overall water splitting under visible light, ACS Catal. 8 (2018) 8649–8658.
[4] H. Li, J. Shang, Z. Ai, L. Zhang, Efficient visible light nitrogen fixation with BiOBr nanosheets of oxygen vacancies on the exposed {001} facets, J. Am. Chem. Soc. 137 (2015) 6393–6399.
[5] J.Y. Li, Z.Y. Zhang, W. Cui, H. Wang, W.L. Cen, G. Johnson, G.M. Jiang, S. Zhang, F. Dong, The spatially oriented charge flow and photocatalysis mechanism on internal van der waals heterostructures enhanced g-C3N4, ACS Catal. 8 (2018) 8376–8385.
[6] L. Zhao, G. Dong, L. Zhang, Y. Lu, Y. Huang, Photocatalytic nitrogen oxide removal activity improved step-by-Step through serial multistep Cu modifications, ACS Appl. Mater. Interfaces 11 (2019) 10042–10051.
[7] J. Kou, C. Lu, J. Wang, Y. Chen, Z. Xu, R.S. Varma, Selectivity enhancement in heterogeneous photocatalytic transformations, Chem. Rev. 117 (2017) 1445–1514.
[8] G. Dong, L. Zhao, X. Wu, M. Zhu, F. Wang, Photocatalysis removing of NO based on modified carbon nitride: the effect of celestite mineral particles, Appl. Catal. B 245 (2019) 459–468.
[9] J. Di, C. Zhu, M. Ji, M. Duan, R. Long, C. Yan, K. Gu, J. Xiong, Y. She, J. Xia, H. Li, Z. Liu, Defect-rich $Bi_{12}O_{17}Cl_2$ nanotubes self-accelerating charge separation for boosting photocatalytic CO_2 reduction, Angew. Chem. Int. Ed. Engl. 57 (2018) 14847–14851.
[10] J. Li, X. Wu, W. Pan, G. Zhang, H. Chen, Vacancy-rich monolayer BiO_{2-x} as a highly efficient UV, visible, and near-infrared responsive photocatalyst, Angew. Chem. Int. Ed. Engl. 57 (2018) 491–495.
[11] Y.G. Zhou, Y.F. Zhang, M.S. Lin, J.L. Long, Z.Z. Zhang, H.X. Lin, J.C.S. Wu, X.X. Wang, Monolayered Bi_2WO_6 nanosheets mimicking heterojunction interface with open surfaces for photocatalysis, Nat. Commun. 6 (2015).
[12] W.C. Huo, Xa. Dong, J.Y. Li, M. Liu, X.Y. Liu, Y.X. Zhang, F. Dong, Synthesis of Bi_2WO_6 with gradient oxygen vacancies for highly photocatalytic NO oxidation and mechanism study, Chem. Eng. J. 361 (2019) 129–138.
[13] N. Zhang, R. Ciriminna, M. Pagliaro, Y.J. Xu, Nanochemistry-derived Bi_2WO_6 nanostructures: towards production of sustainable chemicals and fuels induced by visible light, Chem. Soc. Rev. 43 (2014) 5276–5287.
[14] Y. Lv, W. Yao, R. Zong, Y. Zhu, Fabrication of wide-range-visible photocatalyst Bi_2WO_{6-x} nanoplates via surface oxygen vacancies, Sci. Rep. 6 (2016).
[15] L. Wang, Z.Q. Wang, L.L. Zhang, C. Hu, Enhanced photoactivity of Bi_2WO_6 by iodide insertion into the interlayer for water purification under visible light, Chem. Eng. J. 352 (2018) 664–672.
[16] F. Dong, Z. Zhao, Y. Sun, Y. Zhang, S. Yan, Z. Wu, An advanced semimetal-organic Bi Spheres-g-C_3N_4 nanohybrid with SPR-Enhanced visible-light photocatalytic performance for NO purification, Environ. Sci. Technol. 49 (2015) 12432–12440.
[17] P.E. Blochl, Projector augmented-wave method, Phys. Rev. B 50 (1994) 17953–17979.
[18] G. Kresse, J. Furthmuller, Efficient iterative schemes for ab initio total-energy calculations using a plane-wave basis set, Phys. Rev. B 54 (1996) 11169–11186.
[19] G. Kresse, J. Furthmuller, Efficiency of ab-initio total energy calculations for metals and semiconductors using a plane-wave basis set, Comput. Mater. Sci. 6 (1996) 15–50.
[20] G. Kresse, D. Joubert, From ultrasoft pseudopotentials to the projector augmented-wave method, Phys. Rev. B 59 (1999) 1758–1775.
[21] J.P. Perdew, K. Burke, M. Ernzerhof, Generalized gradient approximation made simple, Phys. Rev. Lett. 77 (1996) 3865–3868.
[22] S. Grimme, Semiempirical GGA-type density functional constructed with a long-range dispersion correction, J. Comput. Chem. 27 (2006) 1787–1799.
[23] V.I. Anisimov, F. Aryasetiawan, A.I. Lichtenstein, First-principles calculations of the electronic structure and spectra of strongly correlated systems: the LDA + U method, Journal of Physics-Condensed Matter 9 (1997) 767–808.
[24] S. Adhikari, D.H. Kim, Synthesis of Bi_2S_3/Bi_2WO_6 hierarchical microstructures for enhanced visible light driven photocatalytic degradation and photoelectrochemical sensing of ofloxacin, Chem. Eng. J. 354 (2018) 692–705.
[25] H.R. Zhou, Z.P. Wen, J. Liu, J. Ke, X.G. Duan, S.B. Wang, Z-scheme plasmonic Ag decorated WO_3/Bi_2WO_6 hybrids for enhanced photocatalytic abatement of chlorinated-VOCs under solar light irradiation, Applied Catalysis B-Environmental 242 (2019) 76–84.
[26] X.Y. Kong, Y.Y. Choo, S.P. Chai, A.K. Soh, A.R. Mohamed, Oxygen vacancy induced Bi_2WO_6 for the realization of photocatalytic CO_2 reduction over the full solar spectrum: from the UV to the NIR region, Chem. Commun. (Camb.) 52 (2016) 14242–14245.
[27] L.Q. Bai, Y.H. Zhang, L.K. Zhang, Y.X. Zhang, L. Sun, N. Ji, X.W. Li, H.C. Si, Y. Zhang, H.W. Huang, Jahn-Teller distortions in molybdenum oxides: an achievement in exploring high rate supercapacitor applications and robust photocatalytic potential, Nano Energy 53 (2018) 982–992.
[28] H. Huang, X. Li, J. Wang, F. Dong, P.K. Chu, T. Zhang, Y. Zhang, Anionic group self-doping as a promising strategy: band-gap engineering and multi-functional applications of high-performance CO32−-doped $Bi_2O_2CO_3$, ACS Catal. 5 (2015) 4094–4103.
[29] K. Hadjiivanov, H. Knözinger, Species formed after NO adsorption and NO + O2 co-adsorption on TiO2: an FTIR spectroscopic study, J. Chem. Soc. Faraday Trans. 2 (2000) 2803–2806.
[30] K. Zha, S. Cai, H. Hu, H. Li, T. Yan, L. Shi, D. Zhang, In situ DRIFTs investigation of promotional effects of tungsten on MnOx-CeO_2/meso-TiO_2 catalysts for NO_x reduction, J. Phys. Chem. C 121 (2017) 25243–25254.
[31] H. Hu, S. Cai, H. Li, L. Huang, L. Shi, D. Zhang, In situ DRIFTs investigation of the low-temperature reaction mechanism over Mn-Doped Co_3O_4 for the selective catalytic reduction of NO_x with NH_3, J. Phys. Chem. C 119 (2015) 22924–22933.
[32] Y. Li, Y. Wan, Y. Li, S. Zhan, Q. Guan, Y. Tian, Low-temperature selective catalytic reduction of NO with NH_3 over Mn_2O_3-Doped Fe_2O_3 hexagonal microsheets, ACS Appl. Mater. Interfaces 8 (2016) 5224–5233.
[33] J.C.S. Wu, Y.-T. Cheng, In situ FTIR study of photocatalytic NO reaction on photocatalysts under UV irradiation, J. Catal. 237 (2006) 393–404.
[34] L. Castoldi, L. Lietti, R. Bonzi, N. Artioli, P. Forzatti, S. Morandi, G. Ghiotti, The NO_x reduction by CO on a Pt−K/Al_2O_3 lean NOx trap catalyst, J. Phys. Chem. C 115 (2011) 1277–1286.
[35] F. Gao, X. Tang, H. Yi, C. Chu, N. Li, J. Li, S. Zhao, In-situ DRIFTS for the mechanistic studies of NO oxidation over α-MnO_2, β-MnO_2 and γ-MnO_2 catalysts, Chem. Eng. J. 322 (2017) 525–537.
[36] J. Mu, X. Li, W. Sun, S. Fan, X. Wang, L. Wang, M. Qin, G. Gan, Z. Yin, D. Zhang, Enhancement of low-temperature catalytic activity over a highly dispersed Fe–Mn/Ti catalyst for selective catalytic reduction of NO_x with NH_3, Ind. Eng. Chem. Res. 57 (2018) 10159–10169.
[37] X. Weng, X. Dai, Q. Zeng, Y. Liu, Z. Wu, DRIFT studies on promotion mechanism of $H_3PW_{12}O_{40}$ in selective catalytic reduction of NO with NH_3, J. Colloid Interface Sci. 461 (2016) 9–14.